Available online at www.sciencedirect.com

ScienceDirect

Procedia CIRP 111 (2022) 662–666

www.elsevier.com/locate/procedia

12th CIRP Conference on Photonic Technologies [LANE 2022], 4-8 September 2022, Fürth, Germany

Secondary electron yield engineering of copper surfaces by 532 nm ultrashort laser pulses

Pierre Lorenz[a,*], Elena Bez[b,c], Marcel Himmerlich[b], Martin Ehrhardt[a], Mauro Taborelli[b], Klaus Zimmer[a]

[a]*Leibniz Institute of Surface Engineering (IOM), Department of ultra-precision surfaces, Permoserstr. 15, 04318 Leipzig, Germany*
[b]*CERN, European Organization for Nuclear Research, 1211 Geneva 23, Switzerland*
[c]*University of Leipzig, Linnéstr. 5, 04103 Leipzig, Germany*

* Corresponding author. Tel.: +49-341-235-3287; *E-mail address:* pierre.lorenz@iom-leipzig.de

Abstract

Nanostructured surfaces exhibit outstanding properties and enable manifold industrial applications. In this study the laser surface processing of polycrystalline, flat copper surfaces by 532 nm picosecond laser irradiation for secondary electron yield (SEY) reduction is reported. The laser beam was scanned in parallel lines across the sample surface in order to modify large surface areas. Morphology and SEY are characterized in dependence of the process parameters to derive correlations and mechanisms of the laser-based SEY engineering process. The nano- and microstructure morphology of the laser-modified surface was characterized by scanning electron microscopy and the secondary electron yield was measured. In general, an SEY reduction with increasing accumulated laser fluence was found. In particular, at low scanning speed (1 mm/s – 10 mm/s) and "high" laser power (~ 1 W) compact nanostructures with a very low SEY maximum of 0.7 are formed.

Keywords: nanostructuring; cooper; laser ablation; secondary electron yield; SEY

1. Introduction

Pulsed laser irradiation of copper surfaces allows the engineering of various surface properties. Pulsed laser irradiation of copper surfaces was studied in dependence on significant laser parameters like pulse duration, laser wavelength, the number of laser pulses, scanning speed, pulse energy, repetition rate [1-17] as well as in dependence on the gas atmosphere [10, 18]. Moreover, the impact of additional external magnetic fields was studied [15]. In addition to the laser ablation pits, nanostructures at and near the ablated copper surface were observed [18]. The resultant micro- and nanoscopic surface morphology depends on the laser parameters [19]. Such hierarchical structured copper surfaces exhibit interesting physical properties such as a low reflectivity [18] and a low secondary electron yield (SEY) [20-25]. Secondary electron emission plays a crucial role for charging phenomena at satellites surfaces, multipacting in radiofrequency devices, and electron cloud formation in particle accelerators like the Large Hadron Collider (LHC) at CERN. Effects of laser-treatment on SEY were studied for copper surfaces using a pulsed laser with a wavelength of λ= 532 nm [22-24]. In this study, the 532 nm picosecond (ps)-laser treatment of copper surfaces was investigated with the aim of a systematic analysis of correlations between the surface morphology and the SEY independence on the laser parameters (scanning speed and laser power).

2. Experimental details

Polycrystalline copper samples with a size of 20×20×1 mm³ were degreased and subsequently passivated in a chromic acid

10.1016/j.procir.2022.08.017

solution. The copper samples were mounted onto a computer-controlled x-y stage. The laser beam (wavelength $\lambda = 532$ nm, pulse duration $\Delta t_p = 12$ ps, repetition rate $f_{rep} = 100$ kHz) was focused by a f-theta lens with a focal length of 165 mm onto the sample surface. A galvo scanner was used for the computer-controlled movement of the laser spot over the sample surface. The laser spot was scanned in parallel lines with a scanning speed ranging from 1 to 200 mm/s and a line distance of $\Delta y = 50$ µm. The scanning procedure is described in detail in [19]. The laser spot had a Gaussian radius of $\omega_0 = (6.4 \pm 2.6)$ µm as determined by Liu's method [26]. The number of laser pulses for a point of the scanned area can be calculated by:

$$N_a = \frac{f_{rep} \cdot 2\omega^2}{\mathbf{v} \cdot \Delta y} \quad (1)$$

and the accumulated laser fluence can be estimated by:

$$\Phi_{acc} = N_a \cdot \frac{P}{f_{rep} \cdot \pi \cdot \omega_0^2} = \frac{P}{\mathrm{v} \cdot \Delta y} \quad (2)$$

The surface topography/morphology of the laser-treated copper surfaces was analysed by scanning electron microscopy (SEM). The secondary electron yield (SEY) was measured on homogenously laser-treated copper samples for primary electron energies between 50 and 1800 eV. More characterization details are described in Ref. [27].

3. Results and Discussion

The morphological characteristics of the laser-exposed, nanostructured copper surface depend on the laser parameters as seen in Fig. 1. The SEM images of the laser-treated surfaces are arranged orthogonally in dependence on the scanning speed v and laser power P. Three different kinds of surface structures dependent on the laser parameter can be distinguished:
(I) Compact nanostructures can be found for the combination of low scanning speed and high or moderate laser power (see Fig. 1 red-marked region). In this case, the accumulated laser fluence is relatively high 3280 – 300 J/cm². Similar compact nanostructures can be produced in experiments with different laser wavelengths [13, 28]. The compact nanostructures can most likely be explained in relation to the redeposition processes of the ablated material.
(II) At moderate scanning speed and moderate laser power (see Fig. 1 green-marked region) the formation of two different kinds of laser-induced periodic surface structures (LIPSS) were detected. LIPSS with a periodicity of ~ 335 nm are almost perpendicular to the laser polarization and LIPSS with a periodicity of ~ 167 nm almost parallel to the laser polarization. The LIPSS structures were found at low accumulated laser fluences in the range between 344 and 48.4 J/cm². The origin of the LIPSS at ~ 335 nm can be explained by the formation of a surface plasmon polariton (SPP) that causes a LIPSS period of (360 ± 20) nm [29]. These structures are oriented perpendicular to the laser polarization. Further, the LIPSS structures are partially covered with sub-µm droplets. The LIPSS at ~167 nm correlated with high spatial frequency laser-induced periodic surface structures (HSFL). The ultra-short pulse laser-induced HSFL was already detected on different metal surfaces [30, 31].

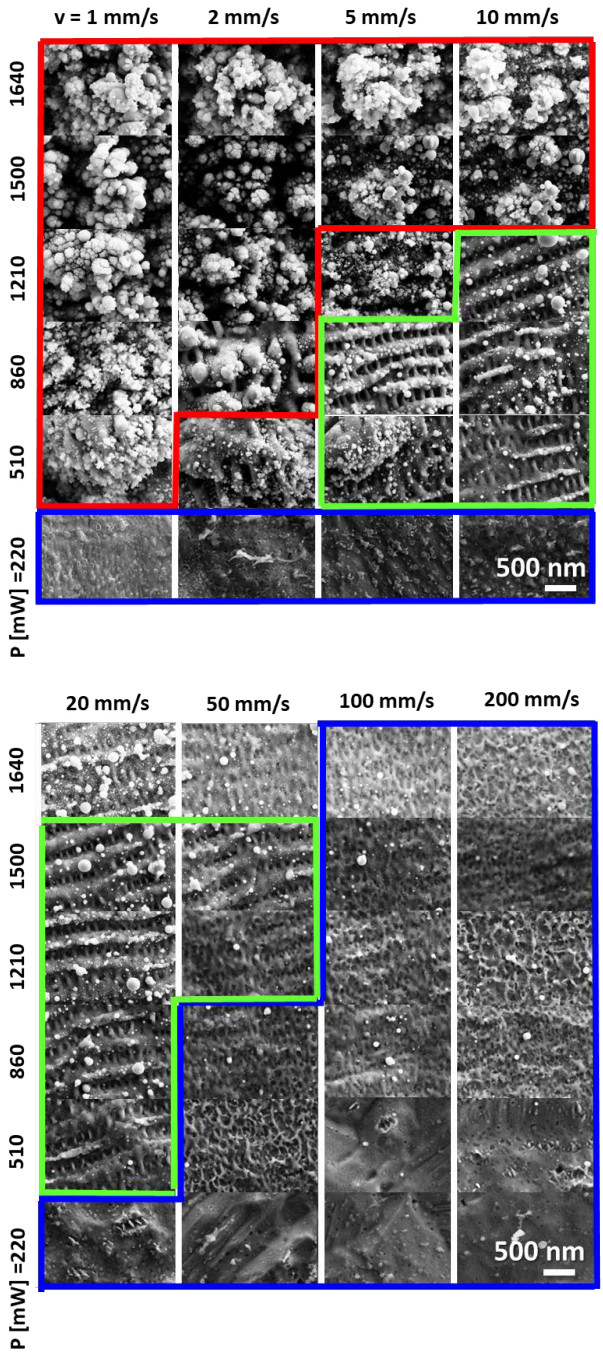

Fig. 1. (a) High-resolution SEM images of copper surface after laser treatment using different laser power P and scanning speed v
(I): red marked region, compact nanostructures
(II) green marked region, laser-induced periodic surface structures
(III) blue marked region, minor modified surface

(III) At higher scanning speeds, generally lower laser powers, and consequently low accumulated laser fluence (between 440 and 2.2 J/cm²), minor modifications like resolidified structures without LIPSS were detected (see Fig. 1 blue-marked region). In conclusion, the parameters laser power and scanning speed strongly influence the resulting surface morphology. The accumulated laser fluence as reference indicates the possible surface topography: with increasing accumulated laser fluence the morphology changes from minor modifications, to LIPSS and to compact nanostructures as long as the ablation threshold fluence is surpassed. According to Calatroni et al. [24] the

multipulse ablation threshold for Cu is 0.42 J/cm² at λ= 532 nm and Δt_p = 10 ps. When varying the scanning speed, both, the number of pulses per unit area and the effective ablation threshold fluence, undergo changes. This effect known as *incubation* as well as other occurring effects limit the projection of the accumulated fluence to the achievable surface morphology. That means, the resultant surface morphology depends complexly on the laser parameter as summarized in Tab. 1.

Table 1. Observed Cu surface structures in dependence on the laser parameters.

Type	high-lighted	structures	Φ_{acc} [J/cm²]	v [mm/s]	P [W]
(I)	red	Compact nanostructures	3280 – 300	1 – 10	1.64 – 0.51
(II)	green	LIPSS	344 – 48.4	5 – 50	1.5 – 0.51
(III)	blue	Minor modified surfaces	440 – 2.2	1 – 200	1.64 – 0.22

The laser-induced morphological, structural, and chemical surface modifications result in an alteration of the interaction of photons and electrons with such surfaces. In Fig. 2 (a), low-resolution secondary electron SEM images of laser-treated copper surfaces at a primary electron energy of 5 keV are shown. The low-resolution SEM images qualitatively include information about the secondary electron emission yield, where the greyscale of the images is representative for the number of emitted secondary electrons (black: low emission, white: high emission) for the actual acceleration voltage. The SEY at 5 keV depends in general on the accumulated fluence, but in more detail the specific processing parameters scanning speed and laser power need to be considered.

The secondary emission is distinctly lower compared to the untreated surface for low scanning speed and high laser power, which is correlated with the existence of compact nanostructures (type I, red marked). The regions which can be correlated to the formation of LIPSS (type II, green marked) show a higher secondary electron emission than the pristine surface at 5 keV. In type III–regions (blue) a slightly higher secondary electron emission compared to the untreated surface is found.

The optical properties – reflectivity for visible light (see Fig. 2 (b)) – of the laser-treated copper surface vary in dependence of the laser processing parameters as well. In general, a strong reflectivity reduction with increasing accumulated fluence is observed. A very low optical reflection is evident for type I (red marked region) morphologies that are dominated by compact nanostructures. Both, the nanostructured surface as well as the microscopic structures (grooves from ablation see e.g. [24]) cause strong scattering effects of the visible light, resulting in the black appearance. Obviously, the nanostructures as well as the microtopography form light trapping surfaces.

Type II patterns (LIPSS, green marked region) lead to a colorful surface. The colors are mainly induced by interference of the illuminating white light (white LED) at the periodic LIPSS features but can be also influenced by the formation of an oxide film.

The reason for the higher reflectivity of type III surfaces (blue marked region) are neither of topographical nor of morphological cause, but can be related to modifications of the near surface region, i.e. chemical alterations (cleaning and passivation) or laser-induced material modifications below the ablation threshold (incubation processes).

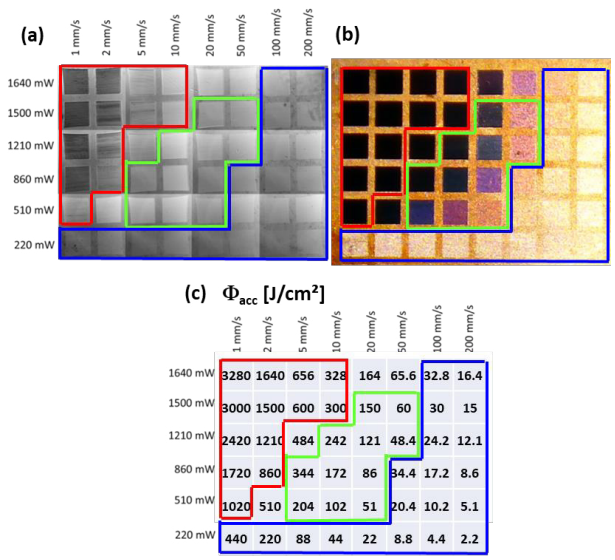

Fig. 2. (a) (left) Low resolution SEM image at a primary electron energy of 5 keV at different scanning speed and laser power
(b) optical image of laser treated copper surface at different scanning speed and laser power (Δy = 50 µm). The SEM parameters during scanning were kept constant.
(c) Accumulated laser fluence Φ_{acc} (based on Eq. 3) dependent on the laser power and scanning speed.

The low-resolution SEM images already highlight the dependence of the SEY at 5 keV on the laser processing parameters. For further analysis, the SEY was determined as a function of the primary electron energy between 50 and 1800 eV for the different laser-modified copper surfaces. In Figure 3 (a), exemplary secondary electron yield curves for different laser parameters are shown. The pristine copper surface (Fig. 3 (a), orange) exhibits a maximum secondary electron yield δ_{max} around 2.1 at a primary electron energy E_p of 250 eV. The laser treatment results in the modification of the shape of the SEY curve as well as in a reduction of the SEY. For example, at Φ_{acc} = 45 J/cm² (Fig. 3 (a) blue curve) the formation of a weakly modified surface results in a SEY maximum δ_{max} = 1.54 eV at E_p = 1200 eV. At Φ_{acc} = 225 J/cm² (Fig. 3 (a) green) the formation of LIPSS results in δ_{max} = 0.91 at E_p = 1800 eV. At Φ_{acc} =3500 J/cm² (Fig. 3 (a) red) the formation of compact nanostructures results in δ_{max} = 0.77 at E_p = 1600 eV. The maximum secondary electron yield δ_{max} in dependence on the accumulated laser fluence Φ_{acc} is summarized in Fig. 3 (b). In general, the δ_{max} decreases with increasing Φ_{acc} and the dependency can be empirically fitted by:

$$\delta_{max} = \delta_{max,th} + \frac{A}{(1+B\cdot\Phi_{acc})^C} \quad (3)$$

with $\delta_{max,th}$ = 0.77, A = 15856, B = 2115 (J/cm²)$^{-1}$ and C = 0.87 (see Fig. 3 (b) grey line).

In disagreement with the formation of the different surface structures which are dependent on the two-dimensional parameter range (P,v), the maximum secondary electron yield presented a correlation to the accumulated laser fluence above 100 J/cm². The reason is probably the increase of the amount of ablated and redeposited material with higher accumulated laser fluences [19]. These redeposits, that are partially modified

by the ongoing laser irradiation, can be considered as the dominating reason for the SEY reduction.

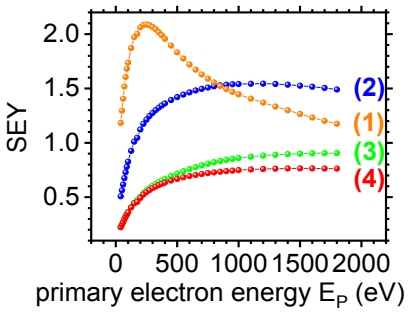

(a)

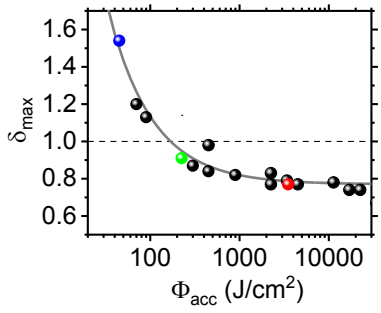

(b)

Fig. 3. (a) Secondary electron yield SEY in dependence of the primary electron energy E_p at different laser parameters:
(1) untreated, δ_{max} = 2.09 at E = 250 eV
(2) (blue) Φ_{acc} = 45 J/cm², v = 15.55 mm/s, Δy = 50 µm, δ_{max} = 1.54 at E = 1200 eV
(3) (green) Φ_{acc} = 225 J/cm², v = 3.11 mm/s, Δy = 50 µm, δ_{max} = 0.91 at E = 1800 eV
(4) (red) Φ_{acc} =3500 J/cm², v = 1 mm/s, Δy = 10 µm, δ_{max} = 0.77 at E = 1600 eV
(b) Maximum secondary electron yield δ_{max} in dependence dependent of the accumulated laser fluence Φ_{acc} (blue/green/red dots: correspond to δ_{max} of the SEY curves summarized in Fig. 4 (a)). Grey curve: data fit using Eq. 3.

4. Conclusion and Outlook

The ps laser ablation of polycrystalline copper surfaces with a laser wavelength of λ = 532 nm leads to the formation of specific surface morphologies that can alter interactions with impinging photons and electrons. Three different kinds of surface nanostructures dependent on the laser parameter were detected: (I) Compact nanostructures induced by a redeposition process were formed at a combination of low scanning speed and high/moderate laser power. (II) LIPSS were formed at moderate scanning speed and moderate laser power induced by self-organized processes. (III) Minor modified surfaces were formed at generally low accumulated laser fluence and induced likely by resolidification processes of the laser melted surface. Specific technical applications call for surface engineering with the goal to reduce the maximum secondary electron yield δ_{max}. The secondary electron yield reduction with increasing accumulated laser fluence was found as a general trend. At low scanning speed (1 – 10 mm/s) and “high” laser power (~ 1 W), compact nanostructures with a very low SEY maximum of 0.7 are formed. The laser-based engineering of surface properties, here shown for SEY reduction of copper, shows excellent potential in a wide range of applications, and can be extended to other materials such as stainless steel and aluminum.

References

[1] Žemaitis A, et al. Highly-efficient laser ablation of copper by bursts of ultrashort tuneable (fs-ps) pulses. Sci Rep, 2019; 9:12280.
[2] Schille J, et al. High-pulse repetition frequency ultrashort pulse laser processing of copper. Journal of Laser Applications, 2015; 27:S28007.
[3] Schille J, et al. Characterisation of interaction phenomena in high repetition rate femtosecond laser ablation of metals. International Congress on Applications of Lasers & Electro-Optics, 2012; 2012:949-958.
[4] Nicolai H, et al., Fundamental investigations of ps-laser burst-mode on common metals for an enhanced ablation process, in: Proc.SPIE, 2015.
[5] Lopez J, et al. Parameters of influence in surface ablation of metals with using a high power tunable ultrafast laser. International Congress on Applications of Lasers & Electro-Optics, 2013; 2013:686-694.
[6] Jordan R, et al. Pulsed laser ablation of copper. Applied Surface Science, 1995; 86:24-28.
[7] Hashida M, et al. Ablation threshold dependence on pulse duration for copper. Applied Surface Science, 2002; 197-198:862-867.
[8] de Rossi W, et al. Effects of ultrashort laser ablation in copper and stainless steel. Lasers in Manufacturing Conference, 2015;
[9] Büttner H, et al. High Aspect Ratio Microstructuring of Copper Surfaces by Means of Ultrashort Pulse Laser Ablation. Procedia CIRP, 2018; 68:190-195.
[10] Bogaerts A, et al. Laser ablation of copper in different background gases: comparative study by numerical modeling and experiments. Journal of Analytical Atomic Spectrometry, 2006; 21:384-395.
[11] Abdelmalek A, et al. Ablation of Copper Metal Films by Femtosecond Laser Multipulse Irradiation. Applied Sciences, 2018; 8:1826.
[12] Zayarny D A, et al. Pulse-width-dependent surface ablation of copper and silver by ultrashort laser pulses. Laser Phys. Lett., 2016; 13:076101.
[13] Yang J, et al. Ablation of metallic targets by high-intensity ultrashort laser pulses. Phys. Rev. B, 2007; 76:165430.
[14] Tunna L, et al. Micromachining of copper using Nd:YAG laser radiation at 1064, 532, and 355 nm wavelengths. Optics & Laser Technology, 2001; 33:135-143.
[15] Pandey P K, et al. Study of pulse width and magnetic field effect on laser ablated copper plasma in air. Physics of Plasmas, 2015; 22:073301.
[16] Mur J, et al. High precision laser direct microstructuring system based on bursts of picosecond pulses. J. Phys. D, 2017; 50:325104.
[17] Bornschlegel B, et al. In-Situ Analysis of Ultrashort Pulsed Laser Ablation with Pulse Bursts. J. Laser Micro/Nanoeng., 2019; 14:7.
[18] Smausz T, et al. Study on the effect of ambient gas on nanostructure formation on metal surfaces during femtosecond laser ablation for fabrication of low-reflective surfaces. Applied Surface Science, 2016; 389:1113-1119.
[19] Lorenz P, et al. Secondary electron yield reduction of copper after 355 nm ultrashort pulse laser ablation. Lasers in Manufacturing and Materials Processing, 2022;
[20] Watts C, et al. Effects of Laser Surface Modification on Secondary Electron Emission of Copper. IEEE Transactions on Plasma Science, 2011; 39:836-841.
[21] Vorobyev A Y, et al. Direct femtosecond laser surface nano/microstructuring and its applications. Laser & Photonics Reviews, 2013; 7:385-407.
[22] Valizadeh R, et al. Low secondary electron yield engineered surface for electron cloud mitigation. Appl. Phys. Lett., 2014; 105:231605.
[23] Calatroni S, et al. First accelerator test of vacuum components with laser-engineered surfaces for electron-cloud mitigation. Physical Review Accelerators and Beams, 2017; 20:113201.
[24] Calatroni S, et al. Cryogenic surface resistance of copper: Investigation of the impact of surface treatments for secondary electron yield reduction. Physical Review Accelerators and Beams, 2019; 22:063101.
[25] Bajek D, et al. Role of surface microgeometries on electron escape probability and secondary electron yield of metal surfaces. Sci Rep, 2020; 10:250-250.

[26] Liu J M. Simple technique for measurements of pulsed Gaussian-beam spot sizes. Opt. Lett., 1982; 7:196-198.
[27] Petit V, et al. Role of the different chemical components in the conditioning process of air exposed copper surfaces. Physical Review Accelerators and Beams, 2019; 22:083101.
[28] Singh S, et al. Effect of ambient air pressure on debris redeposition during laser ablation of glass. J. Appl. Phys., 2005; 98:113520.
[29] Maragkaki S, et al. Wavelength dependence of picosecond laser-induced periodic surface structures on copper. Applied Surface Science, 2017; 417:88-92.
[30] Chen Z, et al. A short review on functionalized metallic surfaces by ultrafast laser micromachining. The International Journal of Advanced Manufacturing Technology, 2022;
[31] Dostovalov A V, et al. LIPSS on thin metallic films: New insights from multiplicity of laser-excited electromagnetic modes and efficiency of metal oxidation. Applied Surface Science, 2019; 491:650-658.